Measurement Simulations of Coupled Qubits with QuTiP

Master Thesis

presented by

Tobias Herrig

submitted to the Faculty of Mathematics, Computer Science and Natural Sciences at RWTH Aachen University

in May 2019

under the supervision of

Prof. Dr. David DiVincenzo
and
Prof. Dr. Fabian Hassler

JARA Institute for Quantum Information

Contents

Abstract

The motivation for this thesis was to investigate if and how it is possible to realize a single-qubit measurement in a system of coupled qubits. The goal was to simulate a homodyne detection on a system with two coupled qubits and a readout resonator and to compare the results to those of Pommerening [10], who approached the same problem analytically with approximations. However, in this thesis we focus on setting up and testing the simulation for the cases of one and two uncoupled qubits, where we expect the homodyne detection to be a projective single-qubit measurement in the computational basis. To do this we solved the Stochastic Schrödinger equation with the *Quantum Toolbox in Python*, or QuTiP, and derived Kraus operators for each measurement outcome. The stochastic schrödinger equation introduces the concept of quantum trajectories, corresponding to single realizations of the measurement. Unfortunately, in the time given and with the computational power provided for this thesis, we could not achieve a satisfactory level of accuracy to apply the simulation on the coupled Hamiltonian.With a larger computational power enabling the calculation of a larger statistical sample, one could possibly reach the target accuracy. Another valuable attempt would be to try all the different stochastic solver methods in the upcoming release of QuTiP 4.4, which are using better approximations than the solver methods that were available in 4.3.

Preliminary Remarks

Background of this work

This thesis is motivated by the work of Pommerening [10]. To be more specific, the analytical method studied by Pommerening is approached here numerically. To this end, we are interested in verifying the validity of the approximations made by Pommerening. For the sake of brevity, the analytical results will not be mentioned, interested readers can refer to Ref. [10] for further details. However, most of the theoretical background in chapters 1 and 2 is based on chapter 4 of Ref. [10] where a proposal on performing a numerical simulation is mentioned.

Notation

In the computational basis, the Pauli matrices are given by

$$X = \begin{pmatrix} 0 & 1 \\ 1 & 0 \end{pmatrix}, \qquad Y = \begin{pmatrix} 0 & -i \\ i & 0 \end{pmatrix}, \qquad Z = \begin{pmatrix} 1 & 0 \\ 0 & -1 \end{pmatrix},$$

where Z has the eigenvalue $\sigma = +1$ for the ground state of a qubit $|0\rangle$ and $\sigma = -1$ for the excited state $|1\rangle$. Because of that, Z appears in the Hamiltonian with a minus sign. The ladder operators are then defined so that $\sigma^+ |0\rangle = |1\rangle$ and $\sigma^- |1\rangle = |0\rangle$. An index usually denotes the qubit, the operator is acting on, while σ will in this thesis always refer to the eigenvalue of Z_1. Note that on the contrary, the usage of Z_1 does not necessarily imply that there is also a second qubit.
The expectation value, according to a certain state $|\psi\rangle$, is denoted throughout the thesis as $\langle \bullet \rangle$, $\langle \bullet \rangle_\psi$ or as $\langle \bullet \rangle_t$, where a subscript of t is referring to a time dependence of the respective state $|\psi(t)\rangle$.
On the contrary, if we are talking about random variables, E[•] and Var[•] will be used for the expectation value and the variance, respectively.

Chapter 1

Introduction

Building a fault-tolerant, scalable quantum computer is not an easy task. One of the DiVincenzo criteria [1] tells us that we need coherence times that are much longer than the time needed for applying one quantum gate. The more qubits in the system, the harder it gets to minimize the decoherence. While quantum error correction (QEC) aims to locate and terminate as many errors as possible, it can only be successful up to a certain rate of errors occurring. Furthermore, there are errors that are uncorrectable or cannot be detected by QEC. Moreover, the QEC can even be faulty by itself. Thus, protection against errors is important to construct a quantum computer.

Errors on qubits may appear, *e.g.*, when applying faulty quantum gates. However, they are primarily induced by the coupling of the qubits to their environment. So one tries to isolate the qubits as much as possible. Of course, they cannot be completely isolated since one still needs an access to measure them or apply gates. Additionally, the qubits have to be coupled to each other in order to facilitate multiqubit gates. Nevertheless, this is a possible source of errors because it is not trivial if or how one can still realize single-qubit gates and measurements on a coupled qubit without causing errors on the other qubits. In this thesis, we want to investigate what happens if we try a single-qubit measurement on a system of coupled qubits. How well can such an operation still be described as a single-qubit measurement? Will it be a projection to a basis of eigenstates and which basis would that be? Let us have a closer look at such a measurement.

A common way to implement measurements on a quantum chip is to couple each qubit to a readout resonator connected to a transmission line. To perform a measurement, the transmission line has to be driven followed by a homodyne or heterodyne detection. But we will not actually model the transmission line, instead we will apply the drive and the measurement directly to the resonator. The homodyne as well as the heterodyne detection is realized by mixing the output signal of the resonator with a reference signal of a strong coherent light field, commonly referred to as local oscillator. The mixing is usually done with a beam splitter. This allows us to obtain information about the phase of the signal, as opposed to a simple photon counting where we only measure the intensity. The difference between homodyne and heterodyne detection is that with homodyne detection the local oscillator has the same frequency as the input drive measuring only one quadrature. With heterodyne detection, on the other hand, the local oscillator has a different frequency measuring

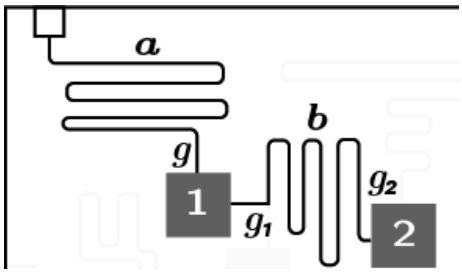

Figure 1.1 – System with two coupled qubits from Ref. [10]. The Boxes are the qubits, which are coupled to the bus resonator $\boldsymbol{b}$ with coupling strengths g_1 and g_2, respectively. The first qubit is also coupled to a readout resonator $\boldsymbol{a}$ with the coupling strength g. The readout resonator is connected to a transmission line for drives and measurements.

two orthogonal quadratures. The quadratures span the optical phase space. In general they look like $x_\phi := \mathrm{e}^{i\phi}a + \mathrm{e}^{-i\phi}a^\dagger$, where a ($a^\dagger$) is the annihilation (creation) operator of the respective oscillator, in our case the readout cavity. The quadratures are often referred to as position and momentum operator of the oscillator as being two hermitian operators orthogonal in the phase space. When measuring the correct quadrature with homodyne detection, there should be no advantage of using heterodyne detection in our case. So for simplicity, we will use homodyne detection.

At first, we will give an introduction to our system and to QuTiP, the software we were using for the simulations. Chapter 2 consists of three parts. First, we will derive the stochastic Schrödinger equation (SSE), which we are going to solve. Secondly, we will define the evolution superoperator based on the solutions of the SSE. This superoperator describes the average evolution conditional on the measurement outcome. In the third part, we present a way to calculate its Kraus representation using a quantum process tomography. In chapter 3 we focus on setting up the simulation. This includes fixing our parameters and a discussion of possible errors, which influence those parameter choices. Furthermore, we will set up tests for the simulation in chapter 4. Finally, in chapter 5 we will present all the results of the simulation, especially of the completeness and linearity tests introduced in the previous chapter. We will also give a short outlook on how future projects could build up on this work and how one could possibly improve the results of the tests further and therefore the precision of the simulation.

1.1 The System

We want to investigate how the coupling of the qubits affects the measurement in a system as simple as possible which still has coupling effects that are non-trivial. So we start with two qubits coupled through a bus resonator, $\boldsymbol{b}$ (see Fig. 1.1). This is the minimal setup for coupled qubits on a quantum chip. Only one of the qubits (qubit 1) is also coupled to a readout resonator, $\boldsymbol{a}$, to allow for a homodyne measurement on this resonator. This system including the following simplifications is the basis for the calculations in the fourth chapter of Ref. [10], where further and more detailed informations can be found.

The inspiring system consists of transmon qubits and capacative couplings to the resonators. However, since we want the Hamiltonian to be as simple as posssible,

we will assume perfect two-level qubits and a Jaynes-Cummings-like interaction as well as resonators with only a single mode. We will subsequently leave out every constant contribution to the Hamiltonian as it will not affect the dynamics of the system. Further information on the implementation of such systems and how to set up the corresponding Hamiltonian can be found in Ref. [2].

The system depicted in Fig. 1.1 has the following Hamiltonian

$$H_0 = \omega_a a^\dagger a + \omega_b b^\dagger b + g\big(a^\dagger \sigma_1^- + a\sigma_1^+\big) + \sum_{i=1}^{2}\left[-\frac{\omega_i}{2}Z_i + g_i\big(b^\dagger\sigma_i^- + b\sigma_i^+\big)\right]. \quad (1.1.1)$$

After a few approximations that can be found in Ref. [10], including a Schrieffer-Wolff transformation, the Hamiltonian can be simplified as follows

$$H_0 = \chi Z_1 a^\dagger a - \frac{1}{2}\sum_{i=1}^{2}\tilde{\omega}_i Z_i + J\big(\sigma_1^+\sigma_2^- + \sigma_1^-\sigma_2^+\big), \quad (1.1.2)$$

where the new constants were defined as follows,

$$\chi = \frac{g^2}{\omega_a - \omega_1}, \qquad \tilde{\omega}_1 = \left(\omega_1 + \frac{g_1^2}{\omega_1 - \omega_b} + \frac{g^2}{\omega_1 - \omega_a}\right),$$
$$\tilde{\omega}_2 = \left(\omega_2 + \frac{g_2^2}{\omega_2 - \omega_b}\right), \qquad J = \frac{g_1 g_2}{2}\left(\frac{1}{\omega_1 - \omega_b} + \frac{1}{\omega_2 - \omega_b}\right).$$

For the homodyne detection on the readout resonator, we need its occupation number to have a non-zero expectation value. Therefore, we add a resonant drive on the readout resonator

$$\epsilon e^{i\omega_a t}a + \epsilon^* e^{-i\omega_a t}a^\dagger \quad \xrightarrow{\text{rotating frame}} \quad \epsilon a + \epsilon^* a^\dagger .$$

Since the resonator was moved to a frame rotating at its resonance frequency ω_a, the driven Hamiltonian looks like

$$H = \chi Z_1 a^\dagger a - \frac{1}{2}\sum_{i=1}^{2}\tilde{\omega}_i Z_i + J\big(\sigma_1^+\sigma_2^- + \sigma_1^-\sigma_2^+\big) + |\epsilon|\big(\mathrm{e}^{i\Phi}a + \mathrm{e}^{-i\Phi}a^\dagger\big), \quad (1.1.3)$$

with $\epsilon = |\epsilon|\mathrm{e}^{i\Phi}$. The dynamics of this Hamiltonian is not exactly solvable due to the coupling term. However, Pommerening has showed that in the uncoupled case ($J = 0$) the steady state solution of the Lindblad master equation for solving Markovian open systems is an eigenstate to Z_1 (with eigenvalue σ) and a coherent state for the resonator

$$|\psi_{ss}\rangle = |\sigma\rangle \otimes |\alpha_\sigma\rangle \qquad \text{with} \qquad \langle x_\Phi\rangle_{\alpha_\sigma} \propto \sigma . \quad (1.1.4)$$

This is an important result because it explains that by doing the homodyne detection in the uncoupled case, we are actually measuring qubit 1 by projecting it to an eigenstate of Z_1 and we get the relevant information by choosing to measure the

correct quadrature in accordance with the applied drive. With that, the actual question of this thesis gets a lot more concrete. How does the measurement differ in the coupled case, *i.e.* for $J \neq 0$? Since Z_1 does not commute with H, the steady state solution can no longer be an eigenstate of Z_1. So what is the new measurement basis? Can we still describe the measurement as a single-qubit measurement and how projective is it?

Pommerening tried to answer these questions using an approximate, analytical approach. We, however, would like to follow a numerical approach to confirm the validity of the analytical results. Unfortunately, a desirable precision was never achieved in the tests of the simulation, which was necessary to investigate the coupled case. Therefore, the only Hamiltonians that were used in the simulations are the ones for only one qubit and for two uncoupled qubits[1]:

$$H_n = \chi Z_1 a^\dagger a - \frac{1}{2}\sum_{i=1}^{n} \tilde{\omega}_i Z_i + \epsilon\big(a + a^\dagger\big)\,, \qquad n \in \{1, 2\}\,, \tag{1.1.5}$$

where ϵ was set to be real, so $\Phi = 0$. In the following, we shall focus on the testing and optimization of the simulation.

1.2 Quantum Toolbox in Python

The simulation runs with the help of the Python package called *Quantum Toolbox in Python*, or in short QuTiP [6]. It is an open source project under permanent development. The current version is 4.4 while I was using 4.2 in the beginning and later 4.3 as soon as it was released in July 2018. It is a framework for the dynamics of open quantum systems and uses other popular python packages like Numpy, Scipy, Cython and Matplotlib. It also provides the new class for all kinds of quantum objects (like states, operators, superoperators...) and many predefined objects as well as tools to manipulate those quantum objects.

[1] A second isolated qubit certainly makes a difference since two uncoupled qubits can still be entangled, depending on the initial state.

Chapter 2

Evolution of the Measurement

A continuous measurement of a system is a stochastic process as it will end up in a different evolution everytime we repeat it. We will describe the single realizations of the measurement in terms of *quantum trajectories*, where each trajectory corresponds to a different path through the Hilbert space. To describe the dynamics of a continuously measured system, we have to consider it as an open system coupled to an environment, often described using a master equation. However, this would give us only the average evolution, independent of the measurement result. To properly calculate possible evolutions, we have to introduce stochastic calculus. This leads us to a stochastic master equation (SME) for potentially mixed states. In our case, all the information leaking out of the system is monitored and no information gets lost, so initally pure states will remain pure during the evolution. Because of that, the SME simplifies to a stochastic Schrödinger equation (SSE) for state vectors making the computation easier. Knowing this, we can derive our SSE directly without the detour over an SME. This rather unusual derivation can be found in more detail in Ref. [3], with Ref. [11] and Ref. [5] providing a more common description of the topic.

2.1 The Wiener Increment

The stochastic calculus will be introduced via the infinitesimal Wiener increment $\mathrm{d}W(t)$. This is a Gaussian random variable with mean 0 and variance $\mathrm{d}t$, while the values at different times are completely independent. With $\mathrm{E}\big[\mathrm{d}W^2\big] = \mathrm{Var}[\mathrm{d}W] = \mathrm{d}t$ and $\mathrm{Var}\big[\mathrm{d}W^2\big]$ being of higher order in $\mathrm{d}t$, we can treat $\mathrm{d}W^2$ as a constant.
So when dealing with those infinitesimal quantities, we will set

$$\mathrm{d}W^2 \to \mathrm{d}t\,, \qquad \mathrm{d}t^2 \to 0\,, \qquad \mathrm{d}W\,\mathrm{d}t \to 0\,. \tag{2.1.1}$$

See Ref. [9] and Ref. [8] for a rather minimalistic discussion of those properties. A more comprehensive treatment of the Wiener process in general can be found in Ref. [11] or Ref. [5].

2.2 Stochastic Schrödinger Equation

In the ideal limit of an infinitely strong local oscillator, homodyne detection will become a continuous, weak measurement. A continuous measurement has a photodetection rate going to infinity, while with a weak measurement, the impact on the system as well as the gain of information for each detection nearly vanishes. Thereby, we can write the evolution of the state vector as a continuous series of weak measurements at every time step between initial time t_0 and time t:

$$|\psi_{\boldsymbol{I}}(t)\rangle = \frac{M_{I_k}(t, t-\mathrm{d}t)...M_{I_1}(t_0+\mathrm{d}t\,, t_0)\,|\psi(t_0)\rangle}{N}\,, \tag{2.2.1}$$

where N is a normalization factor making this equation non-linear. Simultaneously, we are keeping track of the measurement outcomes $I_{n\in[1,k]}$ of every time step forming a sequence $\boldsymbol{I} = [I_1, ..., I_k]$. It determines the quantum trajectory that was taken in the corresponding run of the simulation. Since the time step is infinitesimal, we can equivalently write the outcome sequence as a continuous function of time $J(t)$, which we will call the *measurement current*.

For homodyne detection the infinitesimal measurement operator is

$$M_I(t+\mathrm{d}t\,, t) = \sqrt[4]{\frac{\mathrm{d}t}{2\pi}}\exp\!\left(-\frac{I^2\,\mathrm{d}t}{4}\right)\left(\mathbb{1} - \left[iH(t) - I\sqrt{\kappa}\,\mathrm{e}^{i\Phi}a + \frac{\kappa}{2}a^\dagger a\right]\mathrm{d}t\right), \tag{2.2.2}$$

with the cavity line width κ. This is a complete measurement; the proof of it can be found in the appendix A.1. The respective measurement current can be written as

$$J_{\mathrm{hom}}(t) = \sqrt{\kappa}\langle x_\Phi\rangle_t + \frac{\mathrm{d}W(t)}{\mathrm{d}t}\,, \tag{2.2.3}$$

where the $\frac{\mathrm{d}W}{\mathrm{d}t}$ term introduces white noise around the measured quadrature x_Φ of variance $1/\mathrm{d}t$. The Φ is chosen to be the same as in the driving term in Eq. (1.1.3) allowing to measure the eigenvalue of Z_1 when arriving in the steady state solution as seen in Eq. (1.1.4). A good way to see that Eq. (2.2.2) and (2.2.3) provide a consistent picture of homodyne detection is to derive the probability distribution for the outcome I of a single infinitesimal measurement. See appendix A.2 for the whole calculation.

$$\begin{aligned}\Pr([I], t+\mathrm{d}t) =& \langle M_I^\dagger(t+\mathrm{d}t\,, t)M_I(t+\mathrm{d}t\,, t)\rangle_t \\ =& \sqrt{\frac{\mathrm{d}t}{2\pi}}\exp\!\left(-\frac{\left(I-\sqrt{\kappa}\langle x_\Phi\rangle_t\right)^2\mathrm{d}t}{2}\right)\end{aligned} \tag{2.2.4}$$

This yields a normal distribution with mean $\sqrt{\kappa}\langle x_\Phi\rangle_t$ and variance $1/\mathrm{d}t$, which indeed corresponds to the measurement current $J_{\mathrm{hom}} = \sqrt{\kappa}\langle x_\Phi\rangle_t + \frac{\mathrm{d}W}{\mathrm{d}t}$. From now on, we choose for simplicity $\Phi = 0$, as we have already done in the Hamiltonian.

With the probability distribution, we directly get the normalization constant N for a single time step,

$$N = \sqrt{\langle M_I^\dagger(t+\mathrm{d}t\,, t)M_I(t+\mathrm{d}t\,, t)\rangle_t} = \sqrt{\Pr([I], t+\mathrm{d}t)}\,. \tag{2.2.5}$$

With Eq. (2.2.1), (2.2.2), and (2.2.5), we finally have all the ingredients necessary to derive the SSE,

$$\mathrm{d}|\psi(t)\rangle = |\psi(t+\mathrm{d}t)\rangle - |\psi(t)\rangle = \left\{\frac{M_I(t+\mathrm{d}t\,,t)}{N} - \mathbb{1}\right\}|\psi(t)\rangle$$

$$\Rightarrow \quad \mathrm{d}|\psi(t)\rangle = \left\{-iH\,\mathrm{d}t - \frac{\kappa}{2}\left[a^\dagger a - a\langle a+a^\dagger\rangle_t + \frac{1}{4}\langle a+a^\dagger\rangle_t^2\right]\mathrm{d}t \right.$$
$$\left. + \sqrt{\kappa}\left[a - \frac{1}{2}\langle a+a^\dagger\rangle_t\right]\mathrm{d}W(t)\right\}|\psi(t)\rangle\,. \quad (2.2.6)$$

A detailed derivation can be found in the appendix A.3. If we transformed the SSE into an SME, the corresponding equation for the density operator, and averaged out the stochastic part afterwards, we would end up with the respective Lindblad master equation which was used by Pommerening [10] to derive the steady state solution for the uncoupled case.

2.3 The Evolution Superoperator

The following two sections about the evolution superoperator and the quantum process tomography (QPT) are roughly following the fourth chapter of Pommerening's work [10].

By simulating the SSE, we can now find possible final states for a given initial state. Whenever we do so, we always choose the resonator to start in the vacuum and after computing the final state, we trace out the resonator. Therefore, we only have to care about the state of the qubit(s).
To investigate what the homodyne measurement actually does to an arbitrary initial state (of the qubits), we need to perform a QPT, which allows us to calculate an (super-)operator describing the evolution given the possibility to calculate one final state for every initial state. But since a measurement process inherently involves randomness, we have, in general, more than one possible final state for most initial states. However, we actually want to know the evolution conditional on the total measurement outcome. Hence, we first have to distinguish between the different outcomes and then do a tomography for every one of it after averaging the final state over every quantum trajectory leading to that outcome.

Therefore, we will sort our measured trajectories into several groups, each group standing for a different measurement outcome. And for each of these outcomes we want to calculate a superoperator mapping the initial state to what we will call the *outcome state*. It is the state after the measurement provided the outcome is known and without any knowledge about the specific trajectory that led to the outcome. For a single-qubit measurement we expect there to be two outcomes, which we will refer to with "+" and "−". In the uncoupled case, we expect the measurement current, after averaging out the white noise, to converge to

$$\sqrt{\kappa}\langle x_\Phi\rangle_{\alpha_\sigma} = -\sigma x_{ss}\,, \quad \text{with some} \quad x_{ss} > 0\,. \quad (2.3.1)$$

Hence, we define the two outcomes as the sign of the integral over the measurement current,

$$F^{\pm} := \left\{ \boldsymbol{I} \middle| \int J_{\mathrm{hom}} \, \mathrm{d}t \gtrless 0 \right\}, \tag{2.3.2}$$

with $F^{\pm}$ as the set of all $\boldsymbol{I}$ leading to outcome "$\pm$". When measuring long enough, this definition should indeed coincide with the measurement of $\sigma = \mp 1$ meaning that the qubit ends up to be in the excited state ($\sigma = -1$) for the "+" outcome and the ground state ($\sigma = +1$) for the "$-$" outcome. We will call this criterion the *identification criterion*. In section 3.2 we will discuss whether Eq. (2.3.2) is the optimal way to define the outcomes.

Let us now derive a formula for the outcome state. A full trajectory can be described by a single measurement operator as follows,

$$M_{\boldsymbol{I}} = M_{I_k}(t, t - \mathrm{d}t) ... M_{I_1}(t_0 + \mathrm{d}t \, , t_0) = \prod_{n=1}^{k} M_{I_n} \, . \tag{2.3.3}$$

With that, we can express the final state after one specific trajectory as

$$|\psi_f\rangle = \frac{M_{\boldsymbol{I}} \, |\psi_0\rangle}{\sqrt{\langle \psi_0 | \, M_{\boldsymbol{I}}^{\dagger} M_{\boldsymbol{I}} \, |\psi_0\rangle}} \, . \tag{2.3.4}$$

Now, we average the final state over all trajectories leading to the same outcome, weighted by their probabilities and renormalize afterwards to yield the outcome state and define the superoperator that maps onto it,

$$\mathcal{E}^{\pm}(\rho) := \frac{\sum_{\boldsymbol{I} \in F^{\pm}} M_{\boldsymbol{I}} \rho M_{\boldsymbol{I}}^{\dagger}}{\mathrm{tr}\left(\sum_{\boldsymbol{I} \in F^{\pm}} M_{\boldsymbol{I}}^{\dagger} M_{\boldsymbol{I}} \rho \right)} \, . \tag{2.3.5}$$

This is the so called *evolution superoperator*. However, there are two technical issues for implementing it numerically, as explained in the following. Thus, we make an approximation and redefine Eq. (2.3.5) so that it is suitable for computation.

First of all, we cannot simply simulate every single trajectory for a given initial state, because there are just too many. And there is also not an easy way to calculate their probabilities. However, fortunately, we are only interested in the final states of the trajectories and there are much less different final states than trajectories. So instead, we make use of the law of great numbers by simulating a certain number of random trajectories, *e.g.* $n_{\mathrm{traj}} = 1000$, and average over the obtained final states after separating them according to the outcome criterion. With this, we estimate the probability of a final state by its relative occurence. So we approximate the outcome state by replacing the sum over every trajectory with the sum over a certain number of random trajectories. We will call this approximation the *sampling approximation*.

The second problem is that the superoperator is not linear due to the renormalization. But we need linearity to perform the process tomography, as we will see in the upcoming section. To that end, we will sacrifice the trace-preservation and redefine

the evolution superoperator by removing the renormalization,

$$\tilde{\mathcal{E}}^{\pm}(\rho_0) := \frac{1}{n_{\text{traj}}} \sum \rho_f^{\pm} \,, \tag{2.3.6}$$

where $\rho_f^{\pm}$ is one of the final states of the simulation identified with the "$\pm$" outcome when preparing the initial state ρ_0 and the sum goes over every trajectory in a certain run of the simulation that ends up in this outcome. The trace of this superoperator decreases by a factor that is equal to the rate of those trajectories.

Removing the renormalization would give us initially a linear superoperator but due to the sampling approximation, we will only get approximated linearity. Of course, this will limit the precision of the simulation, as discussed in section 3.1.

2.4 Quantum Process Tomography

The QPT is explained and derived rigorously in the book of Nielsen and Chuang [7]. To know the action of the evolution superoperator on an arbitrary initial state, we do not have to calculate the outcome states for every possible initial state but only for a basis of operators, due to the linearity. For a Hilbert space of size d, we need d^2 independent operators in our basis. Considering an N-qubit system, we naturally start with the $d = 2^N$ states of the computational basis $|n\rangle\langle n|$, where we can just apply $\tilde{\mathcal{E}}^{(\pm)}$. One might go on with the operators $|n\rangle\langle m|$ for $n \neq m$ but we cannot prepare them as initial states since $\rho = |n\rangle\langle m|$ is not a physical state. Instead, we will write them as a linear combination of physical states

$$|n\rangle\langle m| = |+\rangle\langle +|_{nm} + i\,|-\rangle\langle -|_{nm} - \frac{1+i}{2}\,|n\rangle\langle n| - \frac{1+i}{2}\,|m\rangle\langle m| \,, \tag{2.4.1}$$

with $n \neq m$ and

$$|+\rangle_{nm} = \frac{|n\rangle + |m\rangle}{\sqrt{2}} \,, \qquad |-\rangle_{nm} = \frac{|n\rangle + i\,|m\rangle}{\sqrt{2}} \,. \tag{2.4.2}$$

Because now, we can use the linearity of our superoperator again to consistently define

$$\tilde{\mathcal{E}}(|n\rangle\langle m|) := \tilde{\mathcal{E}}(|+\rangle\langle +|_{nm}) + i\tilde{\mathcal{E}}(|-\rangle\langle -|_{nm}) - \frac{1+i}{2}\tilde{\mathcal{E}}(|n\rangle\langle n|) - \frac{1+i}{2}\tilde{\mathcal{E}}(|m\rangle\langle m|) \,. \tag{2.4.3}$$

However, we now have in total more than d^2 initial states corresponding to operators in our basis, so we do not need all of them. We can just restrict $n < m$ and use the adjoint version of Eq. (2.4.1)

$$|m\rangle\langle n| = |+\rangle\langle +|_{nm} - i\,|-\rangle\langle -|_{nm} - \frac{1-i}{2}\,|n\rangle\langle n| - \frac{1-i}{2}\,|m\rangle\langle m| \,, \tag{2.4.4}$$

which leaves us with the d states $|n\rangle$, the $d(d-1)/2$ states $|+\rangle_{n<m}$ and the same number of the states $|-\rangle_{n<m}$ adding up to d^2 states we have to prepare.

With applying $\tilde{\mathcal{E}}$ to these states, we can already fully characterize it. Nevertheless, we want a useful representation of the superoperator. Our goal is to derive a Kraus representation of $\tilde{\mathcal{E}}$,

$$\tilde{\mathcal{E}}(\rho) = \sum_{i=1}^{d^2} \widetilde{M}_i \, \rho \, \widetilde{M}_i^{\dagger} \ . \tag{2.4.5}$$

Here it is important to note that these Kraus operators $\widetilde{M}_i$ are not the same as the $M_{\boldsymbol{I}}$ defined in Eq. (2.3.3). While there is one $M_{\boldsymbol{I}}$ for every possible trajectory, there are only d^2 Kraus operators. To calculate those, we will first consider a different representation by choosing a fixed set of operators $\{E_i\}$ forming a basis for the operators acting on ρ, so that we can write

$$\widetilde{M}_i = \sum_j e_{ij} E_j \, . \tag{2.4.6}$$

It is convenient to choose the identity and the Pauli matrices or respectively tensor products of those as the basis $\{E_i\}$. This gives us the *chi matrix representation*

$$\tilde{\mathcal{E}}(\rho) = \sum_{j,k} E_j \rho E_k^{\dagger} \chi_{jk} \, , \tag{2.4.7}$$

with

$$\chi_{jk} := \sum_i e_{ij} e_{ik}^{*} \, . \tag{2.4.8}$$

This representation shows that a linear superoperator can be fully described by a Hermitian $d^2 \times d^2$-matrix, χ, once the operator basis $\{E_i\}$ is fixed.

Fortunately, the Python package we are using for the simulation, QuTiP, has an in-built function which transforms a superoperator from its matrix representation acting on vectorized matrices into its χ matrix representation. Hence, we write the superoperator in the vectorized form as

$$|\tilde{\mathcal{E}}(\rho)\rangle\rangle = U \, |\rho\rangle\rangle \, , \tag{2.4.9}$$

where

$$|\rho\rangle\rangle = \sum_{i,j} \rho_{ij} \, |i\rangle \otimes |j\rangle \, , \qquad \text{for} \qquad \rho = \sum_{i,j} \rho_{ij} \, |i\rangle\langle j| \, . \tag{2.4.10}$$

We can compute U with

$$U_{ij} = \langle\langle \rho_i | \tilde{\mathcal{E}}(\rho_j) \rangle\rangle = \mathrm{tr}\Big(\rho_i^{\dagger} \tilde{\mathcal{E}}(\rho_j) \Big) \, . \tag{2.4.11}$$

where we have defined

$$\rho_{n \cdot d + m + 1} := |n\rangle\langle m| \, , \qquad n, m \in [0, d-1] \, . \tag{2.4.12}$$

Once we know χ, we can directly calculate the Kraus operators by diagonalizing χ

$$\chi_{jk} = \sum_i u_{ji} d_i u_{ki}^* \,. \tag{2.4.13}$$

And by comparing Eq. (2.4.13) with Eq. (2.4.8), we get

$$\widetilde{M}_i = \sqrt{d_i} \sum_j u_{ji} E_j \,. \tag{2.4.14}$$

Finally, we have a protocol on how to calculate the Kraus operators for the evolution superoperator if we have the possibility to calculate final states for any given initial state. To do this in a proper and physically relevant way, we need to discuss the following technical details.

Chapter 3

Technical Details

The task is now to take care of the technical details, like fixing the parameters, in such a way that the results are physically meaningful and can represent actual physical processes. At the same time, we want to minimize the possible errors that increase the linearity violation of the evolution superoperator. We will try to do so for the (both one and two) uncoupled qubits case because there we can identify those errors rather easily, since we know the optimal result as opposed to the coupled qubits case. Afterwards we can just adopt the setting for the latter.

The used QuTiP versions provided two different methods to solve stochastic differential equations (SDE), *Euler-Maruyama* and *Platen*. The Euler-Maruyama method generalizes the Euler method for ordinary differential equations to stochastic differential equations and was used to produce all the data for this thesis. The Platen method was, in comparison, more time consuming without resulting in a better precision. Even though QuTiP 4.4 is currently still in development, it will contain many more solver methods, like *e.g. Milstein* or *Runge-Kutta*. These approximations are valid to higher orders, so that those methods are worth considering for future projects.

3.1 Parameter Choices

To set up a working simulation, it is important to fix the parameters in a reasonable way. We start with those appearing in the Hamiltonian and the SSE (Eq. (1.1.5) and (2.2.6)), namely $\chi, \tilde{\omega}_1, \tilde{\omega}_2, \epsilon, \kappa$, which all have dimensions of energy. We will fix those parameters by setting them in proportion to χ, whose fixing will then set the energy scale as well as the time scale. A realistic value for χ from experimental systems is around 0.5-1.0 MHz (in terms of a non-angular frequency)[1]. Realistic values for parameters in typical systems are discussed in Ref. [2]. Nevertheless, for simplicity we just set χ to 1, or equivalently, we choose the energy units u_E to be around 0.5-1.0 MHz $\cdot\, h$, where h is the Planck constant. Then this just fixes the units of time u_t to 160-320 ns. Hence, if we speak about values of time, we will call it for instance $1\,[u_t]$, which translates to a value around 160-320 ns. This analogously applies to values of energy in terms of $u_E = u_t^{-1}$. This also means that the measurement current has units of $\sqrt{u_E}$.

[1]Note that we are using natural units so far, *i.e.* $\hbar = 1$.

We also have to introduce another important parameter, namely the size of the resonator Hilbert space N. Numeric simulations cannot handle infinite dimensions of vector spaces; therefore, the question arises which states to keep in the truncated space. It is convenient to take the Fock basis and just cut the Hilbert space at a certain photon number N, while keeping the states closer to the vacuum. Of course, the removed states should have negligible occupation to not cause problems. Regardless, a larger Hilbert space always means larger computing times and a larger memory needed.

Looking at the two steady state solutions (according to the two values of σ), we can maximize the phase space separation

$$|\alpha_+ - \alpha_-| = \frac{2|\epsilon\chi|}{\frac{\kappa^2}{4} + \chi^2} \tag{3.1.1}$$

by setting

$$\kappa = 2\chi\,, \tag{3.1.2}$$

which should lead to a better distinction between the two outcomes (see Ref. [10]). We also notice that the separation is proportional to ϵ. So a stronger input drive also gives us a clearer measurement and less errors due to a false identification of trajectories, meaning assigning them the wrong outcome. On the contrary, with a larger ϵ we would also need a larger Hilbert space since a stronger field implies a higher occupation number $n = \langle a^\dagger a \rangle$. In the steady state, we would have

$$n_{\alpha_\sigma} = |\alpha_\sigma|^2 = \frac{\epsilon^2}{\frac{\kappa^2}{4} + \chi^2}\,, \tag{3.1.3}$$

so we expect a good value for N to be proportional to that – at least approximately, because it has to be an integer – and larger. Indeed, a few tests yielded that in the end,

$$\epsilon = 3\chi \qquad \text{and} \qquad N = 4n_{\alpha_\sigma} + 2 \tag{3.1.4}$$

turns out to be a reasonable choice.

In the one-qubit case, we can always move the qubit to a frame rotating at its resonance frequency, so we can just set $\tilde{\omega}_1 = 0$ without any physical relevance. For two qubits we can only set one of the frequencies to zero since the two qubits should be in the same frame in order to not change the coupling term in the Hamiltonian (Eq. (1.1.3)). So we need a physically sensible value for the difference of the frequencies, for example around 100 MHz. Hence, we set

$$\tilde{\omega}_1 = 100\chi \qquad \text{and} \qquad \tilde{\omega}_2 = 0\,. \tag{3.1.5}$$

Actually, every attempt to fix those in a different way with $\tilde{\omega}_2$ being non-zero resulted in the expectation value of Z_2 converging very slowly to $+1$ or -1 depending on the sign of $\tilde{\omega}_2$. Very slowly means here on a scale much longer than the average collapse time, which is the time until an eigenstate of Z_1 is reached. To be perfectly clear, we are talking about the uncoupled case, so this is really something unphysical, which should not happen. Due to time constraints, we were not able to investigate

this more closely. Even though we can avoid that effect by choosing $\tilde{\omega}_2 = 0$, it is still a hint that maybe the solver of the SSE is not working precise enough for our calculations.

The last parameter we are going to fix now is the number of substeps in the solver of the SSE. To really understand what those substeps are, one has to understand how the solver method works, which we will not discuss here. The important thing to know is that those substeps are steps that are taken within one time step. So we want a value that is as low as possible as it increases the computation time while still being not too low that it causes errors or an unphysical behavior. A few tests showed that

$$n_{\text{substeps}} = N \tag{3.1.6}$$

is an appropriate choice.

The parameters we are now left with are those strongly affecting the computation time and possibly also the needed memory. To find optimal values for them, we will look at several tests of the simulation which are varying these parameters to reduce certain errors.

- First of all, there is the **measurement time** T_{meas}, the time difference between the start and the end of the measurement. If this is too low, there will be errors due to not yet collapsed states, collapsed meaning projected to one of the two steady states. Then the identification of the corresponding outcome will be rather arbitrary, just like the final state of that trajectory. So it should be much larger than the average collapse time of the trajectories.

- Then there is the **time step** $\mathrm{d}t$. It should be much smaller than any other time scale, since only then, we expect a physical behavior of the trajectories. On the other hand, the simulation can get very expensive if $\mathrm{d}t$ is too small.

- The last parameter is the **number of trajectories** n_{traj} used for every initial state when calculating the superoperator. Since we are using the law of great numbers with the sampling approximation, the relative frequency of an outcome will mostly not coincide with its probability for a given initial state, but it should be a better approximation the more trajectories we take into account. On the other hand, with more trajectoies, we expext there to be in total more problematic trajectories, which could be accounted for with a longer measurement time.

  In fact, we can actually estimate the induced error. If we simulate n_{traj} trajectories for an equal superposition between the two eigenstates of Z_1 as initial state, we can describe the number of trajectories identified with outcome "+" with a binomial distribution of probability $p = 50\%$. We are assuming 100% collapsed states and no false identifications. The relative standard deviation for this distribution is

$$\sigma_{\text{rel}}(n_{\text{traj}}) = \sqrt{\frac{p(1-p)}{n_{\text{traj}}}} = \frac{1}{2\sqrt{n_{\text{traj}}}}\,. \tag{3.1.7}$$

So, for example, we get

$$\sigma_{\text{rel}}(100) = 5\%\,, \quad \sigma_{\text{rel}}(1000) = 1.58\%\,, \quad \text{and} \quad \sigma_{\text{rel}}(10^4) = 0.5\%\,. \tag{3.1.8}$$

3.2 Identification Criterion

Whether Eq. (2.3.2) is the optimal way to define the outcomes is not obvious; one may think of alternatives to optimize the evaluation of the simulation results. For example one may average the measurement current over an intermediate timescale and define the outcomes by the sign of the last value of that average, so that early times do not influence the assignment. Another idea would be to introduce a threshold J_{min} so that one assigns a trajectory to an outcome only if the absolute value of the averaged or integrated measurement current lies above the threshold. Otherwise the trajectory would not be taken into account. This, on the one hand, may reduce the errors by sorting out inconclusive or non-collapsed trajectories. On the other hand, we may also throw away trajectories that were actually not problematic, which may then lead to higher errors since we would have less trajectories to analyze for the same computational input. Which of those effects the more dominant is depends on the rate of problematic trajectories.

Choosing a good identification criterion is a crucial factor to reduce the number of false identifications, which refers to the trajectories that are already collapsed to an eigenstate of Z_1 but identified with the opposite outcome. The frequency of this error also depends on the strength of the input drive ϵ, as already mentioned, and the measurement time T_{meas}, thanks to the regression to the mean. So, what we can do is to choose a measurement time that is long enough to reduce the number of all problematic trajectories, the false identified as well as the non-collapsed, to a minimum so that the proposed alternative criteria would not improve the results or even worsen them. See Ref. [4] for more information on how the measurement time affects the fidelity of the outcome identification.

Chapter 4

Tests of the Simulation

4.1 Calculating χ

For the case of one qubit, Nielsen and Chuang [7] have laid out a concrete way of calculating the χ matrix. We can use it to check the QuTiP function. They chose the operator basis

$$E_0 = \mathbb{1}\,, \qquad E_1 = X\,, \qquad E_2 = -iY\,, \qquad E_3 = Z\,.$$

Then one can calculate χ directly with

$$\chi = \Lambda \begin{pmatrix} \rho_1' & \rho_2' \\ \rho_3' & \rho_4' \end{pmatrix} \Lambda\,, \qquad \text{where} \qquad \Lambda := \frac{1}{2}\begin{pmatrix} \mathbb{1} & X \\ X & -\mathbb{1} \end{pmatrix} \quad \text{and} \quad \rho_i' := \tilde{\mathcal{E}}(\rho_i)\,, \quad (4.1.1)$$

in terms of block matrices. One should be aware that the χ matrix depends on the chosen basis. Hence, to compare those with different bases, we will transform it first into its Kraus representation. Nevertheless, we then still have to be careful because the Kraus representation is only determined up to unitary transformations.

It turns out that the two methods of calculating χ lead to exactly the transposed Kraus representation, which may be just an undetected typo in the code. However, this does not impair the following two tests, since a transposition does not increase any errors.

4.2 Linearity of the Evolution Superoperator

Linearity is a very important condition for the QPT to work and due to the sampling approximation, it only holds approximately. We can test the quality of this apprzoximation by computing the linearity of the superoperator. To test the linearity we use the identity

$$|-\rangle\langle -|_{nm} + |-\rangle\langle -|_{mn} = |n\rangle\langle n| + |m\rangle\langle m|\,, \quad (4.2.1)$$

where the $|-\rangle_{nm}$ states were defined in Eq. (2.4.2). This relation can be derived by combining Eq. (2.4.1) and (2.4.4). Using this relation, we can construct the following

linearity condition:

$$\tilde{\mathcal{E}}(|-\rangle\langle-|_{nm}) + \tilde{\mathcal{E}}(|-\rangle\langle-|_{mn}) \stackrel{?}{=} \tilde{\mathcal{E}}(|n\rangle\langle n|) + \tilde{\mathcal{E}}(|m\rangle\langle m|)\,. \tag{4.2.2}$$

To check it, we have to calculate the outcome state of the initial state $|-\rangle_{n>m}$, meaning $\tilde{\mathcal{E}}\big(|-\rangle\langle-|_{n>m}\big)$, because it is not in our operator basis for the QPT. For one qubit there is only one such state $|-\rangle_{10}$. In the case of two qubits, we choose the states $|-\rangle_{10}$ and $|-\rangle_{30}$, where

$$\{|0\rangle\,,\,|1\rangle\,,\,|2\rangle\,,\,|3\rangle\} := \{|00\rangle\,,\,|01\rangle\,,\,|10\rangle\,,\,|11\rangle\}\,.$$

To have a quantitative measure for the linearity violation of the superoperator, we define the quantity

$$\lambda = \|\Lambda\|_1\,, \tag{4.2.3}$$

with

$$\Lambda = \tilde{\mathcal{E}}(|-\rangle\langle-|_{nm}) + \tilde{\mathcal{E}}(|-\rangle\langle-|_{mn}) - \tilde{\mathcal{E}}(|n\rangle\langle n|) - \tilde{\mathcal{E}}(|m\rangle\langle m|)\,. \tag{4.2.4}$$

Here we have used the trace norm

$$\|\Lambda\|_1 := \mathrm{tr}\,\sqrt{\Lambda\Lambda^\dagger}\,. \tag{4.2.5}$$

To distinguish λ for the different states, we add indices to it, so that λ_1 corresponds to the one-qubit case and $\lambda_{2,1}$ and $\lambda_{2,2}$ correspond to the two-qubit states $|-\rangle_{10}$ and $|-\rangle_{30}$, respectively. We will try to minimize those quantities in the tests of the simulation.

Since the two-qubit state $|-\rangle_{10}$ is an eigenstate of Z_1, we expect the only randomness in its outcome state to be in the occurrence of false identifications. Therefore, $\lambda_{2,1}$ represents the rate of false identifications. The linearity check for the state $|-\rangle_{30}$ corresponds to the one-qubit test but with an entangled state, so it might give different results.

4.3 Completeness of Kraus Representation

In order to obtain, at least approximately, linear evolution superoperators, we had to sacrifice the trace preservation of both $\tilde{\mathcal{E}}^+$ and $\tilde{\mathcal{E}}^-$, which now depends on both the input state and coincidence. Nevertheless, we still have trace preservation for the sum of both superoperators

$$\mathrm{tr}\Big(\tilde{\mathcal{E}}^+(\rho_0) + \tilde{\mathcal{E}}^-(\rho_0)\Big) = \frac{1}{n_{\mathrm{traj}}}\sum \mathrm{tr}(\rho_f) = \mathrm{tr}(\rho_0)\,, \tag{4.3.1}$$

where we are summing over all the n_{traj} trajectories of the respective run. The last equation only holds true if the final states produced by the simulation are indeed normalized, but the QuTiP solver for the SSE explicitly takes care of that. The trace preservation is equivalent to a completeness relation for the Kraus operators, which can be derived by inserting the Kraus representation into the left side of the

above equation,

$$\sum_i \left(\widetilde{M}_{-,i}^\dagger \widetilde{M}_{-,i} + \widetilde{M}_{-,i}^\dagger \widetilde{M}_{-,i} \right) = \mathbb{1} + \Delta \,, \tag{4.3.2}$$

where Δ is the error due to the lack of linearity. Linearity is a requirement not only for the QPT but also in general to be able to write a superoperator in the Kraus representation. So another rather indirect test of linearity is provided via the quantity

$$\delta = \frac{\|\Delta\|_1}{d} = \frac{\mathrm{tr}(\Delta)}{d} \,, \tag{4.3.3}$$

where $d = 2^{n_q}$ is the Hilbert space dimension of the n_q qubits in our system. Due to the factor of $1/d$, we get a quantity that is actually a good approximation for the biggest occurring error in the Kraus operators, compared to perfect projectors to the corresponding "+" or "−" eigenstate.

Analogously to the linearity test, we add indices, defining δ_1 and δ_2 for one and two qubits, respectively.

The linearity and the completeness checks are the main tests of the simulation, which we use to find optimal values for the remaining parameters. Their results are discussed in the following chapter.

Chapter 5

Results

5.1 Simulation of the Trajectories

When the measured qubit starts in an eigenstate of Z_1, the evolution is stationary and not stochastic at all[1]. The much more interesting cases are where the measured qubit is in an equal superposition of $|0\rangle$ and $|1\rangle$ or in a state entangled with the second qubit. So we primarily investigate evolutions of these initial states in the following. Also, it often does not make a difference whether we are talking about one or two (uncoupled) qubits; many statements are applicable to both cases.

As an experimentalist who is measuring a qubit with homodyne detection, we would receive just the measurement current as an output signal. See Fig. 5.1 for an example of such a signal. Since the stochastic part, with variance $\mathrm{d}t^{-1}$, is usually much larger than the deterministic part, we need to average the signal, at least over an intermediate timescale, to obtain information over the quadrature term and therefore over the state of the measured qubit. The connection of these two is best seen when comparing Fig. 5.3 and Fig. 5.4, which visualize the expectation values of $-Z_1$ and of the quadrature $\sqrt{\kappa}x$ for the same five trajectories. While $-\langle Z_1\rangle_t$ reaches an eigenvalue $\sigma = \pm 1$, which corresponds to the expected projection, the quadrature term reaches its steady state value, which confirms the theoretic prediction[2] [10],

$$\sqrt{\kappa}\langle x\rangle_{\alpha_\sigma} = \frac{2\epsilon\sqrt{\kappa}\chi}{\frac{\kappa^2}{4}+\chi^2} = 3\sqrt{2}\,[\sqrt{u_E}] \approx 4.24\,[\sqrt{u_E}]\,. \tag{5.1.1}$$

The evolution of two qubits that are initially maximally entangled is depicted in Fig. 5.2. It shows that the expectation values of Z_1 and Z_2 are up to a minus sign always the same during the evolution.

We can also estimate the average collapse time from those figures to be roughly around $1.0\,[u_t]$ to $1.5\,[u_t]$. This gives us a first hint of how large the measurement time has to be to avoid non-collapsed states.

[1] Of course, this may not be true anymore if we would turn on the coupling between the qubits.

[2] Looking closely at Fig. 5.4, one can observe that the absolute value at $t = 3\,[u_t]$ is actually a bit higher than $4.24\,[\sqrt{u_E}]$. Nevertheless, for larger times, it falls back and approaches the steady state solution from above.

A nice way to see how many false identifications there are in a run of the simulation is to make a histogram that shows the number of trajectories leading to a certain value of the integrated measurement current like Fig. 5.5 or Fig. 5.6. If this measurement integral has the same sign as the expectation value of Z_1, we call it a false identification, even though this does not make sense if we are talking about a non-collapsed state. In that case to bring sense to it, we are just guessing the outcome $\sigma = \pm 1$ of a non-collapsed state with $\langle Z_1 \rangle_{T_{\text{meas}}} \gtrless 0$. Fig. 5.5 shows a histogram of a run with 1000 trajectories and a measurement time of $1.5\,[u_t]$ or $2.5\,[u_t]$, respectively. These distributions have a Gaussian-like shape similar to the prediction, which can be found for example in Ref. [10]. Now, we still have an overlap of those distributions for $T_{\text{meas}} = 1.5\,[u_t]$, which indicates that we should either optimize our identification criterion or increase the measurement time. However, for a time of $2.5\,[u_t]$ and larger, there is no overlap anymore, at least in most runs since there is always a slight chance of a false identification. This may also not be true anymore when increasing the sample size to more than 1000 trajectories. Therefore, $2.5\,[u_t]$ should be a reasonable measurement time. For interested readers, Ref. [4] provides a discussion of the fidelity of such measurement protocols as ours, including the dependence on the measurement time. In Fig. 5.6, we have a histogram for 100 trajectories but with a measurement time of $3.0\,[u_t]$. The fact that these distributions are not really Gaussian-like indicates that a sampling of a hundred trajectories is not really representative, unlike a sample with a thousand trajectories.

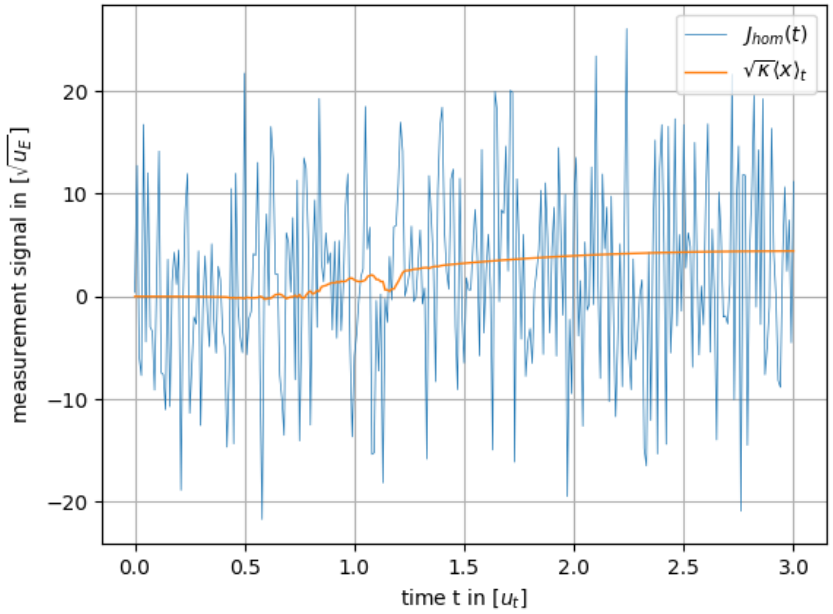

Figure 5.1 – Measurement current with and without the stochastic part as a function of time. The measurement current is the signal we measure during a homodyne detection. Without the stochastic part, this is just the quadrature term $\sqrt{\kappa}\langle x\rangle_t = \sqrt{\kappa}\langle a + a^\dagger\rangle_t$, and the stochastic term $\frac{\mathrm{d}W}{\mathrm{d}t}$ is white noise of variance $1/\mathrm{d}t$. Here, we have $\mathrm{d}t = 10^{-2}\,[u_t]$. The unit of time u_t is around 160-320 ns and the unit of energy $u_E = u_t^{-1}$.

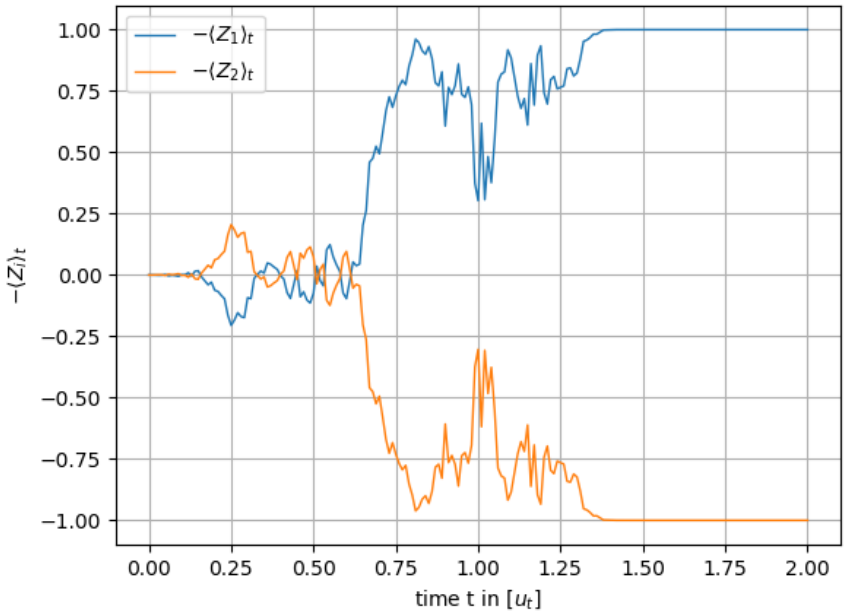

Figure 5.2 – Expectation values of $-Z_1$ and $-Z_2$ as functions of time during a measurement with the maximally entangled initial state $(|01\rangle + |10\rangle)/\sqrt{2}$. Due to the minus signs, a final value of -1 corresponds to the ground state of the according qubit. The unit of time is around 160-320 ns. The time step is here $\mathrm{d}t = 10^{-2}\,[u_t]$. At every point in time the expectation value of Z_1 is exactly the expectation value of $-Z_2$.

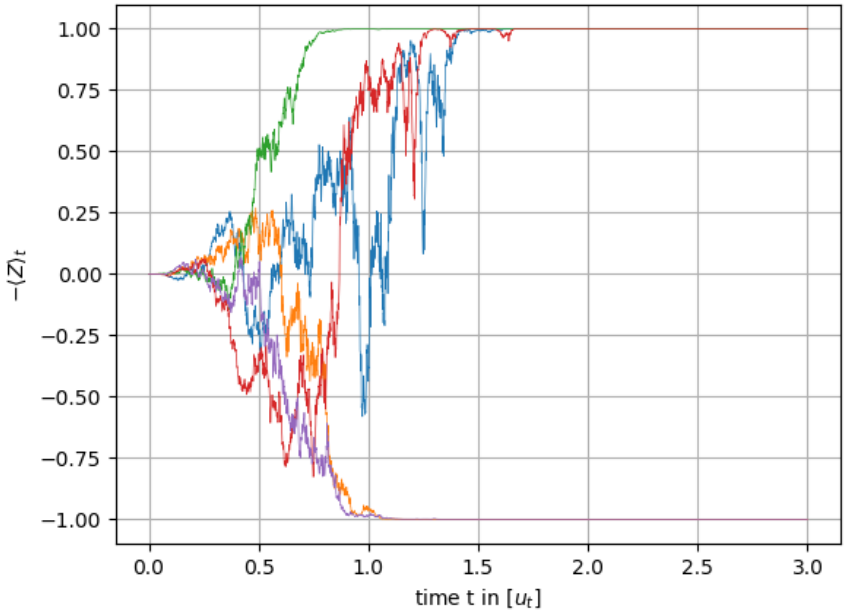

Figure 5.3 – Expectation value of $-Z$ as a function of time during the measurement of a single qubit for five quantum trajectories. Due to the minus sign, a final value of -1 corresponds to the ground state. The unit of time u_t is around 160-320 ns. The initial state is here $(|0\rangle + |1\rangle)/\sqrt{2}$ and the time step $\mathrm{d}t = 10^{-3}\,[u_t]$. After the state has collapsed, it stays an eigenstate of Z with eigenvalue $\sigma = \pm 1$. A rough estimate of the average collapse time would be around 1.0-1.5 $[u_t]$.

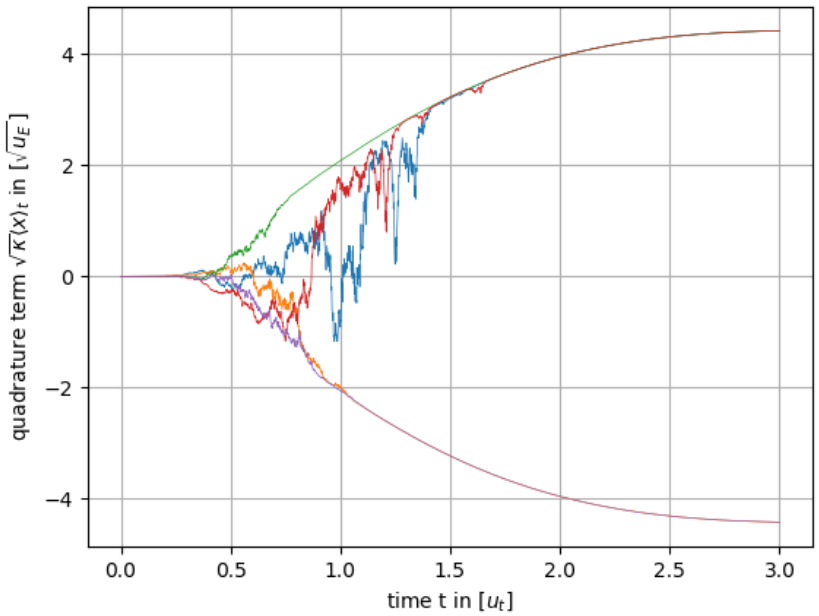

Figure 5.4 – Expectation value of the measured quadrature term $\sqrt{\kappa}\langle x\rangle_t = \sqrt{\kappa}\langle a + a^\dagger\rangle_t$ for the same quantum trajectories as in Fig. 5.3 . The unit of time u_t is around 160-320 ns and the unit of energy $u_E = u_t^{-1}$. After the state has collapsed into an eigenstate of Z, the quadrature term becomes a smooth function of time. For large times, it approaches one of the two steady state values $\pm 3\sqrt{2}\,[\sqrt{u_E}] \approx \pm 4.24\,[\sqrt{u_E}]$.

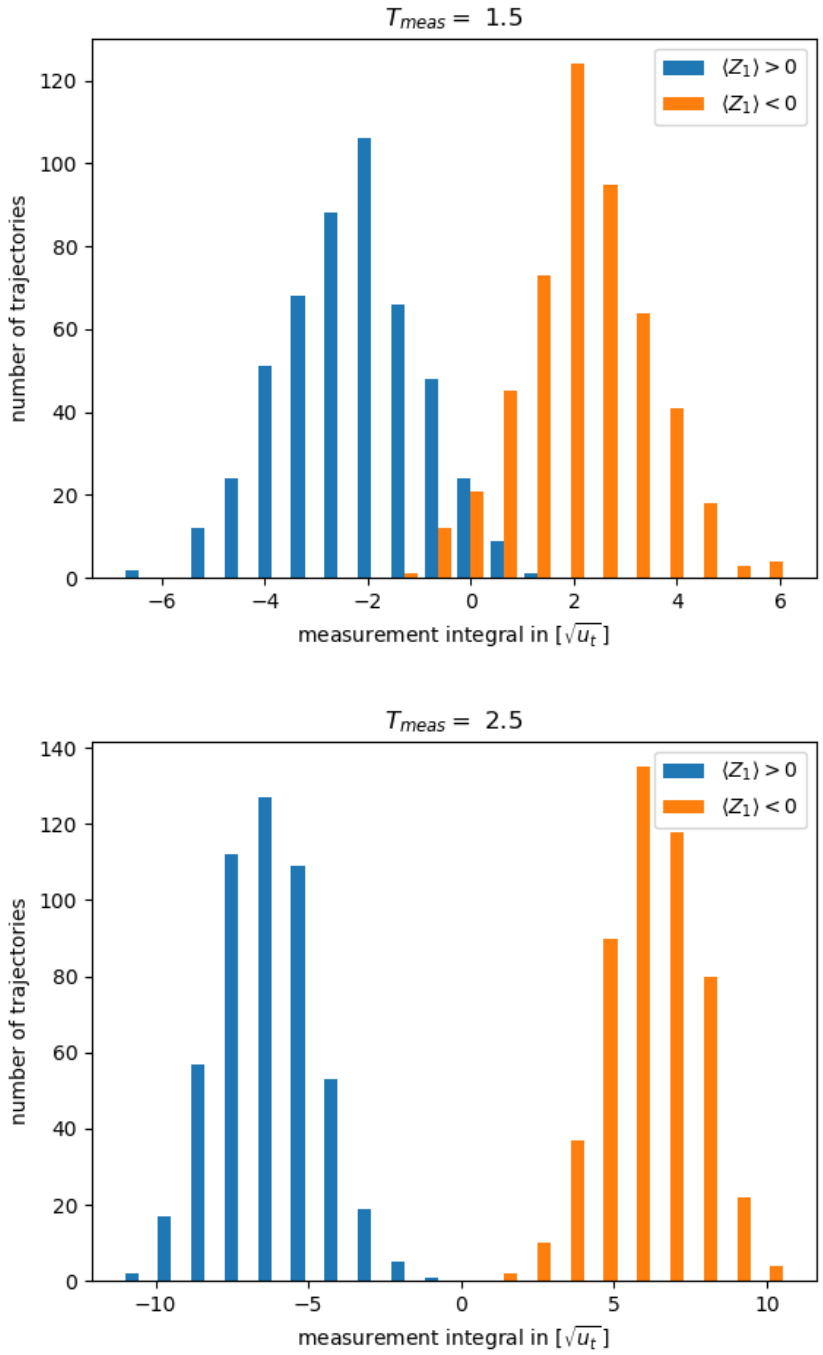

Figure 5.5 – Histogram for the integrated measurement currents with 1000 trajectories in total. Blue indicates a positive expectation value of Z_1 at the final time $T_{\text{meas}} = 1.5\,[u_t]$ or $T_{\text{meas}} = 2.5\,[u_t]$, respectively, while orange indicates a negative one. Here, the time step was chosen to be $\mathrm{d}t = 10^{-2}\,[u_t]$ and the initial state is $(|0\rangle + |1\rangle)/\sqrt{2}$. The histograms show the distribution of how many trajectories of an actual outcome $\sigma = \pm 1$ end up with a certain value for the integrated measurement current. It represents the fidelity of the identification criterion since it shows how many false identifications happened. We treat non-collapsed states with $\langle Z_1 \rangle_{T_{\text{meas}}} \gtrless 0$ as belonging to $\sigma = \pm 1$, meaning that we guess to which state it would have collapsed if T_{meas} had been larger. The overlap of the two distributions is what we want to avoid by choosing a better identification criterion or a higher measurement time. The measurement time of $2.5\,[u_t]$ is an appropriate lower bound, at least for the sample size of 1000 trajectories, in order to avoid false identifications.

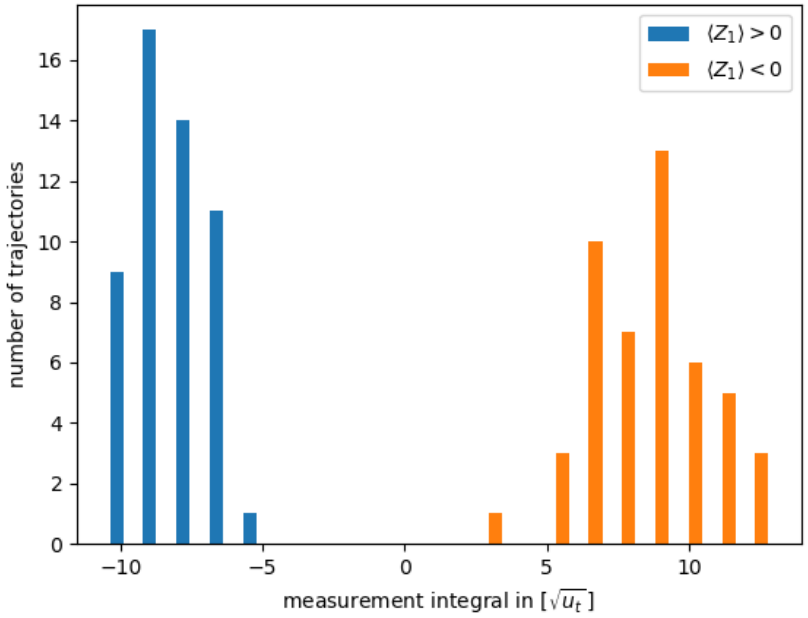

Figure 5.6 – Histogram for the integrated measurement currents with 100 trajectories in total. Blue indicates a positive expectation value of Z_1 at the final time $T_{\text{meas}} = 3.0\,[u_t]$ while orange indicates a negative one. Here, the time step was chosen to be $\mathrm{d}t = 10^{-2}\,[u_t]$ and the initial state is $(|0\rangle + |1\rangle)/\sqrt{2}$. Analogous to Fig. 5.5, the histogram shows the distribution of how many trajectories of an actual outcome $\sigma = \pm 1$ end up with a certain value for the integrated measurement current. The higher measurement time, compared to Fig. 5.5, shifts those distributions further apart, removing all the false identifications. Due to the lower total number of trajectories, the distributions are looking less like a Gaussian.

5.2 Completeness and Linearity Condition

Let us now have a look at the results of the linearity and the completeness checks. The time step does not influence the results of these tests in an recognizable way, as long as the step size is not larger than $\mathrm{d}t = 10^{-2}\,[u_t]$. This is why the values for different step sizes are bunched together in the following tables. Each interval combines five results for $\mathrm{d}t$ between $10^{-2}\,[u_t]$ and $10^{-4}\,[u_t]$. Of course, this is not enough to have a statistically meaningful range but it gives us at least a rough estimate. We start with $n_{\mathrm{traj}} = 100$ trajectories, while the measurement time varies from $0.1\,[u_t]$ to $3.0\,[u_t]$.

n_{traj}	$T_{\mathrm{meas}}/[u_t]$	$100 \cdot \lambda_1$	$100 \cdot \delta_1$	$100 \cdot \lambda_{2,1}$	$100 \cdot \lambda_{2,2}$	$100 \cdot \delta_2$
100	0.1	$\sim$ 5.0-19	$\sim$ 4.5-16	$\sim$ 2.8-16	$\sim$ 3.0-15	$\sim$ 22-52
	0.3	$\sim$ 6.1-18	$\sim$ 9.7-15	$\sim$ 4.0-17	$\sim$ 3.0-16	$\sim$ 23-45
	0.5	$\sim$ 2.7-19	$\sim$ 1.9-15	$\sim$ 4.2-19	$\sim$ 7.0-10	$\sim$ 21-37
	0.7	$\sim$ 5.0-15	$\sim$ 1.5-3.8	$\sim$ 4.0-17	$\sim$ 2.7-23	$\sim$ 22-40
	1.0	$\sim$ 3.2-15	$\sim$ 1.1-3.8	$\sim$ 6.0-13	$\sim$ 4.0-17	$\sim$ 22-25
	1.5	$\sim$ 2.3-12	$\sim$ 0.88-5.8	$\sim$ 2.2-5.4	$\sim$ 4.0-12	$\sim$ 11-16
	2.0	$\sim$ 1.0-12	$\sim$ 0.26-2.9	~ 0 [3]-1.0	$\sim$ 1.0-9.0	$\sim$ 7.5-13
	2.5	$\sim$ 1.0-12	$\sim$ 0.18-1.8	0 [3]	$\sim$ 3.0-7.0	$\sim$ 6.6-13
	3.0	$\sim$ 0.0003-9.0	$\sim$ 0.10-1.0	0 [3]	$\sim$ 1.0-10	$\sim$ 4.2-13

Table 5.1 – Results of the linearity and the completeness checks for 100 trajectories. The value ranges correspond to five bundled up values for $\mathrm{d}t$ between $10^{-2}\,[u_t]$ and $10^{-4}\,[u_t]$.

First of all, most of these values are not very small but they are decreasing when going to a higher measurement time until about $2.0\,[u_t]$. This is not surprising since we have a lot of non-collapsed states and also a higher rate of false identifications for low measurement times. The quantities λ_1, δ_1, $\lambda_{2,1}$ and $\lambda_{2,2}$ are all in the same range for lower T_{meas}, while δ_1 decreases faster for an increasing measurement time and $\lambda_{2,1}$ just drops to zero[3] rather quickly around $T_{\mathrm{meas}} \approx 2.0\,[u_t]$. That $\lambda_{2,1}$ is dropping to zero indicates that we have almost certainly no false identifications[4] for measurement times larger than $2.0\,[u_t]$, which confirms the similar statement based on the histograms. However, what is really standing out here is that the values of δ_2 are conspicuously larger for all values of T_{meas}. This is probably due to the fact that the size of the density matrix increases by a factor of four when going from the one-qubit to the two-qubit space, while the two qubits are in general not separable.

Let us at this point recall the estimation of the error due to the sampling approximation (see Eq. (3.1.8)):

$$\sigma_{\mathrm{rel}}(100) = 5\%\,, \qquad \sigma_{\mathrm{rel}}(1000) = 1.58\%\,, \qquad \sigma_{\mathrm{rel}}(10^4) = 0.5\%\,. \tag{5.2.1}$$

[3]The zero values are exactly zero since an eigenstate of Z_1 gets mapped to itself by the superoperator, as long as there are no false identifications, and in that case the linearity condition becomes trivial.

[4]It is only almost certainly because there is always a slight chance that a false identification will happen anyways when repeating the simulation.

Basically, we expect this error to scale with $1/\sqrt{n_{\text{ntraj}}}$. Additionally, the errors due to problematic trajectories should average out to some extend when the number of trajectories increases. Hence, we will now look at the results for $n_{\text{traj}} = 1000$ in the next table.

In this table, there are four results bundled up for each interval with dt between $10^{-2}\,[u_t]$ and $3.3 \cdot 10^{-4}\,[u_t]$.

n_{traj}	T_{meas}	$100 \cdot \lambda_1$	$100 \cdot \delta_1$	$100 \cdot \lambda_{2,1}$	$100 \cdot \lambda_{2,2}$	$100 \cdot \delta_2$
1000	0.1	$\sim$ 2.5-5.1	$\sim$ 3.4-5.6	$\sim$ 1.7-5.2	$\sim$ 0.5-3.2	$\sim$ 5.8-16
	0.3	$\sim$ 2.5-6.3	$\sim$ 0.89-5.1	$\sim$ 2.7-6.9	$\sim$ 2.2-7.4	$\sim$ 9.1-15
	0.5	$\sim$ 2.2-4.9	$\sim$ 0.37-2.6	$\sim$ 2.8-5.2	$\sim$ 1.2-4.0	$\sim$ 5.9-12
	0.7	$\sim$ 1.7-10	$\sim$ 0.31-1.7	$\sim$ 2.6-5.4	$\sim$ 1.9-5.2	$\sim$ 6.5-12
	1.0	$\sim$ 1.2-4.1	$\sim$ 0.35-0.73	$\sim$ 1.0-4.7	$\sim$ 1.2-4.5	$\sim$ 5.5-9.9
	1.5	$\sim$ 0.99-2.5	$\sim$ 0.093-0.39	$\sim$ 1.0-1.7	$\sim$ 1.0-2.3	$\sim$ 4.2-6.0
	2.0	$\sim$ 0.19-1.4	$\sim$ 0.19-0.50	$\sim$ 0.2-0.8	$\sim$ 1.4-4.8	$\sim$ 2.4-4.2
	2.5	$\sim$ 0.20-2.4	$\sim$ 0.024-0.17	0	$\sim$ 0.10-1.6	$\sim$ 2.0-4.0
	3.0	$\sim$ 0.40-3.4	$\sim$ 0.036-0.22	0	$\sim$ 0.70-3.6	$\sim$ 2.3-3.4

Table 5.2 – Results of the linearity and the completeness checks for 1000 trajectories. The value ranges correspond to four bundled up values for dt between $10^{-2}\,[u_t]$ and $3.3{\cdot}10^{-4}\,[u_t]$.

Most values did indeed decrease roughly by a factor of $\sqrt{0.1}$. The values for δ_1, which represents the error size in the Kraus operators for the one-qubit case, are now at a satisfactory level. Nevertheless, we are primarily interested in the two-qubit errors, which are still significantly higher and not at all satisfying. So do we just need more trajectories? When keeping in mind that those values are only a sample of four values and are therefore not providing a reliable upper limit, we probably would have to increase the number of trajectories at least by a factor of 100. However, a number of 10^5 trajectorieswould cost a lot of computation time and memory. During the work on this project it was a recurring issue to reduce the needed memory, because the QuTiP source code for this solver was not optimized in that regard. And even though methods to parallelize the computation of the different trajectories were used as much as possible with the given resources, the simulations were still relatively expensive in both computation time and needed memory. So increasing the number of trajectories by another factor of 100 was not a reasonable option with the given resources.

5.3 Summary & Outlook

In this thesis we have explained a way to describe the evolution of continuous measurements and how to simulate such a process. We have obtained an SSE that allows us to compute final states. Afterwards, we defined the evolution superoperator to help us understand the process and explained a way how to calculate its Kraus representation using a QPT. To distinguish the final states according to their measurement outcome, we had to find a identification criterion. We also have discussed possible errors in such a simulation, namely falsely identified states and not yet collapsed states on the other hand. However, the error that turned out to be the biggest hurdle was due to the sampling approximation, which we needed to be able to calculate the superoperator. To minimize these errors, we thought about the optimal ways on how to fix the relevant parameters. Finally, we have constructed tests of the simulation checking the linearity of the superoperator and the completeness of the Kraus representation and tried to optimize the simulation with the help of those tests.

We have done all this while considering the uncoupled case because we know its solution. To consider the coupled case, it was necessary to have an error that is small enough, so that the effects of the coupling on the Kraus operators would be dominant. However, due to the limited resources and time for the project we never achieved that goal, so we leave that to future projects. Maybe, if one had more computational power and could significantly reduce the needed memory, one could try simulations with 10^5 trajectories. However, it might be possible to reduce the errors with a different way. For instance, one should definitely try different solvers for the SSE. As already mentioned, it was announced that there will be many new solver methods in the next release of QuTiP (version 4.4). This alone could already improve the results since there are many solvers with better approximations in their methods. At least the issue, that the results behaved unphysical for $\tilde{\omega}_2 \neq 0$ is definitly a hint that there is something not working that well, which may be due to the solver method.

As a final remark, one has to be careful when doing simulations of stochastic processes. On the one hand, it is often recommendable or even necessary to repeat certain runs of the simulations, because it is valuable to have a feeling for the variability of the obtained results. Furthermore, there are no random numbers in a simulation. Therefore, one has to be very careful that the pseudorandom number generator (PRNG) is producing numbers that are "random enough", meaning that the statistics are close enough to that of actually random numbers. One also has to take care that the PNRG is seeded properly and at every necessary point, especially, when using parallelization methods.

Bibliography

[1] David P. DiVincenzo. The physical implementation of quantum computation. *Fortschritte der Physik: Progress of Physics*, 48(9-11):771–783, 2000. URL: https://arxiv.org/abs/quant-ph/0002077.

[2] J. M. Gambetta. Control of superconducting qubits. In David P. DiVincenzo, editor, *Quantum Information Processing: Lecture Notes of the 44th IFF Spring School*, volume 52 of *Schlüsseltechnologien/Key Technologies*. Schriften des Forschungszentrums Jülich, 2013.

[3] J. M. Gambetta. *Non-Markovian Stochastic Schrödinger Equations and Interpretations of Quantum Mechanics*. PhD thesis, Griffith University, Sept 2003. URL: https://www120.secure.griffith.edu.au/rch/file/cbbaebc1-353c-615b-586b-ae25cc7abf06/1/02Whole.pdf.

[4] Jay Gambetta, W. A. Braff, A. Wallraff, S. M. Girvin, and R. J. Schoelkopf. Protocols for optimal readout of qubits using a continuous quantum nondemolition measurement. *Physical Review A*, 76(1):012325, 2007. DOI: https://doi.org/10.1103/PhysRevA.76.012325.

[5] C. W. Gardiner and P. Zoller. *Quantum noise: a handbook of Markovian and non-Markovian quantum stochastic methods with applications to quantum optics*. Springer, 2004.

[6] J. Robert Johansson, Paul D. Nation, and Franco Nori. Qutip 2: A python framework for the dynamics of open quantum systems. *Computer Physics Communications*, 184(4):1234–1240, 2013. DOI: https://doi.org/10.1016/j.cpc.2012.11.019.

[7] Michael A. Nielsen and Isaac L. Chuang. *Quantum Computation and Quantum Information: 10th Anniversary Edition*. Cambridge University Press, 2010. DOI: https://doi.org/10.1017/CBO9780511976667.

[8] D. S. G. Pollock. Continuous-time processes. Lecture Notes: EC3070 Financial Derivatives, Leicester University. URL: https://www.le.ac.uk/users/dsgp1/COURSES/DERIVATE/FINADERV.html.

[9] D. S. G. Pollock. Ito's lemma. Lecture Notes: EC3070 Financial Derivatives, Leicester University. URL: https://www.le.ac.uk/users/dsgp1/COURSES/DERIVATE/FINADERV.html.

[10] J. C. Pommerening. Multiqubit coupling dynamics and the cross-resonance gate. Master's thesis, RWTH Aachen University, Sept

2017. URL: `https://www.quantuminfo.physik.rwth-aachen.de/global/show_document.asp?id=aaaaaaaaaaxokfj`.

[11] H. M. Wiseman and G. J. Milburn. *Quantum Measurement and Control*. Cambridge University Press, 2010.

Appendix A

Calculations to derive the SSE

Before we start the derivation, In those calculations it is important to be careful if one is not used to the properties of the Wiener increment (see Eq. (2.1.1)). Let us recall them shortly: we consequently set

$$\mathrm{d}W^2 \to \mathrm{d}t\,, \qquad \mathrm{d}t^2 \to 0\,, \qquad \mathrm{d}W\,\mathrm{d}t \to 0\,. \tag{A.0.1}$$

The measurement outcome as an instance of the measurement current is

$$I = \sqrt{\kappa}\langle x_\Phi\rangle + \frac{\mathrm{d}W}{\mathrm{d}t}\,. \tag{A.0.2}$$

Together with the "rules" from above, we directly get

$$(I\,\mathrm{d}t)^2 = \left(\sqrt{\kappa}\langle x_\Phi\rangle\,\mathrm{d}t + \mathrm{d}W\right)^2 = \mathrm{d}t\ , \tag{A.0.3}$$

where the equality is only valid up to orders of $\mathrm{d}W\,\mathrm{d}t$ and $\mathrm{d}t^2$. It should be said that in the following calculations, the equality sign is understood that Eq. (A.0.1) might have to be applied to obtain actual equality. We will repeatedly use either Eq. (A.0.1), Eq. (A.0.3) or the following relation,

$$\exp(x) = 1 + x + \frac{x^2}{2} + \mathcal{O}\big(x^3\big) \tag{A.0.4}$$

with x either of order $\mathrm{d}W$ or $\mathrm{d}t$.

A.1 Completeness of Infinitesimal Measurement Operator

We start with the infinitesimal measurement operator [3],

$$M_I(t+\mathrm{d}t\,,t) = \sqrt[4]{\frac{\mathrm{d}t}{2\pi}}\exp\left(-\frac{I^2\,\mathrm{d}t}{4}\right)\left(\mathbb{1} - \left[iH(t) - I\sqrt{\kappa}\,\mathrm{e}^{i\Phi}a + \frac{\kappa}{2}a^\dagger a\right]\mathrm{d}t\right). \tag{A.1.1}$$

From this, it is easy to see that $M_I^\dagger M_I$ can be written in the form

$$M_I^\dagger M_I = \sqrt{\frac{\mathrm{d}t}{2\pi}} \exp\!\left(-\frac{I^2\,\mathrm{d}t}{2}\right)\left(A + BI + CI^2\right), \tag{A.1.2}$$

where A, B and C are some operators that are independent of I. So we can calculate the integral

$$\begin{aligned}\mathcal{I} :=& \int_{-\infty}^{\infty} \mathrm{d}I\, M_I^\dagger(t+\mathrm{d}t\,,t) M_I(t+\mathrm{d}t\,,t)\\ =&\sqrt{\frac{\mathrm{d}t}{2\pi}} \int_{-\infty}^{\infty} \mathrm{d}I \exp\!\left(-\frac{I^2\,\mathrm{d}t}{2}\right)\left(A + BI + CI^2\right)\\ =&\frac{1}{\sqrt{\pi}} \int_{-\infty}^{\infty} \mathrm{d}x\, \mathrm{e}^{-x^2}\left(A + \sqrt{\frac{2}{\mathrm{d}t}}Bx + \frac{2}{\mathrm{d}t}Cx^2\right),\end{aligned} \tag{A.1.3}$$

where we made the substitution $x := I\sqrt{\mathrm{d}t/2}$. Now, we have basically three integrals to solve. The first one is just the Gaussian integral,

$$\int_{-\infty}^{\infty} \mathrm{d}x\, \mathrm{e}^{-x^2} = \sqrt{\pi}\,.$$

The second integral is zero,

$$\int_{-\infty}^{\infty} \mathrm{d}x\, x\mathrm{e}^{-x^2} = 0\,,$$

since we are integrating an odd function over an even interval. And the third integral we solve with integration by parts,

$$\int_{-\infty}^{\infty} \mathrm{d}x\, x^2\mathrm{e}^{-x^2} = -\frac{x}{2}\mathrm{e}^{-x^2}\Big|_{-\infty}^{\infty} + \frac{1}{2}\int_{-\infty}^{\infty} \mathrm{d}x\, \mathrm{e}^{-x^2} = \frac{\sqrt{\pi}}{2}\,.$$

All together, we get

$$\Rightarrow \quad \mathcal{I} = A + \frac{C}{\mathrm{d}t}\,. \tag{A.1.4}$$

Now, we just need to calculate A and C,

$$\begin{aligned}M_I^\dagger M_I =&\sqrt{\frac{\mathrm{d}t}{2\pi}} \exp\!\left(-\frac{I^2\,\mathrm{d}t}{2}\right)\left(\mathbb{1} - \left[-iH(t) - I\sqrt{\kappa}\,\mathrm{e}^{-i\Phi}a^\dagger + \frac{\kappa}{2}a^\dagger a\right]\mathrm{d}t\right)\\ &\times\left(\mathbb{1} - \left[iH(t) - I\sqrt{\kappa}\,\mathrm{e}^{i\Phi}a + \frac{\kappa}{2}a^\dagger a\right]\mathrm{d}t\right)\\ =&\sqrt{\frac{\mathrm{d}t}{2\pi}} \exp\!\left(-\frac{I^2\,\mathrm{d}t}{2}\right)\left(\mathbb{1} - \kappa a^\dagger a\,\mathrm{d}t + H^2(t)\,\mathrm{d}t^2 + \frac{\kappa^2}{4}\left(a^\dagger a\right)^2\mathrm{d}t^2\right.\\ &\left.+ BI + I^2\kappa a^\dagger a\,\mathrm{d}t\right),\end{aligned} \tag{A.1.5}$$

where all the terms proportional to I are contained in the BI term. We can identify

$$A = \mathbb{1} - \kappa a^\dagger a \,\mathrm{d}t + H^2(t)\,\mathrm{d}t^2 + \frac{\kappa^2}{4}\big(a^\dagger a\big)^2\,\mathrm{d}t^2 \quad \text{and} \quad C = \kappa a^\dagger a \,\mathrm{d}t^2 \ .$$

Thus, we can conclude

$$\int_{-\infty}^{\infty} \mathrm{d}I\, M_I^\dagger(t+\mathrm{d}t\,,t) M_I(t+\mathrm{d}t\,,t) = A + \frac{C}{\mathrm{d}t} = \mathbb{1} + \mathcal{O}\big(\mathrm{d}t^2\big), \tag{A.1.6}$$

so the infinitesimal measurement defined by Eq. (A.1.1) is a complete measurement up to orders of $\mathrm{d}t^2$.

A.2 Probability Distribution of Measurement Outcome

Now, we want to derive the probability distribution for the outcome I of a single infinitesimal measurement. In this calculation we mainly connect terms linear in $\mathrm{d}t$ with terms quadratic in $I\,\mathrm{d}t$ through Eq. (A.0.3) and use Eq. (A.0.4) to bring it in an exponential form,

$$\begin{aligned}
\Pr([I], t+\mathrm{d}t) =& \langle M_I^\dagger(t+\mathrm{d}t\,,t) M_I(t+\mathrm{d}t\,,t)\rangle_t \\
=& \sqrt{\frac{\mathrm{d}t}{2\pi}} \exp\!\left(-\frac{I^2\,\mathrm{d}t}{2}\right) \left\langle \left(\mathbb{1} + \left[I\sqrt{\kappa}\mathrm{e}^{-i\Phi} a^\dagger - \frac{\kappa}{2} a^\dagger a\right]\mathrm{d}t\right) \right. \\
& \left. \times \left(\mathbb{1} + \left[I\sqrt{\kappa}\mathrm{e}^{i\Phi} a - \frac{\kappa}{2} a^\dagger a\right]\mathrm{d}t\right)\right\rangle_t \\
=& \sqrt{\frac{\mathrm{d}t}{2\pi}} \exp\!\left(-\frac{I^2\,\mathrm{d}t}{2}\right) \left(1 + \left[\sqrt{\kappa}\langle x_\Phi\rangle_t I - \kappa\langle a^\dagger a\rangle_t\right]\mathrm{d}t + \kappa\langle a^\dagger a\rangle_t (I\,\mathrm{d}t)^2\right) \\
=& \sqrt{\frac{\mathrm{d}t}{2\pi}} \exp\!\left(-\frac{I^2\,\mathrm{d}t}{2}\right) (1 + \langle x_\Phi\rangle_t I\,\mathrm{d}t) \\
=& \sqrt{\frac{\mathrm{d}t}{2\pi}} \exp\!\left(-\frac{I^2\,\mathrm{d}t}{2}\right) \left(1 + \left[\langle x_\Phi\rangle_t I\,\mathrm{d}t - \frac{1}{2}\langle x_\Phi\rangle_t^2\,\mathrm{d}t\right] + \frac{1}{2}\langle x_\Phi\rangle_t^2 (I\,\mathrm{d}t)^2\right) \\
=& \sqrt{\frac{\mathrm{d}t}{2\pi}} \exp\!\left(-\frac{I^2\,\mathrm{d}t}{2}\right) \exp\!\left(\langle x_\Phi\rangle_t I\,\mathrm{d}t - \frac{1}{2}\langle x_\Phi\rangle_t^2\,\mathrm{d}t\right) \\
=& \sqrt{\frac{\mathrm{d}t}{2\pi}} \exp\!\left(-\frac{I^2\,\mathrm{d}t}{2} + \langle x_\Phi\rangle_t I\,\mathrm{d}t - \frac{1}{2}\langle x_\Phi\rangle_t^2\,\mathrm{d}t\right) \\
=& \sqrt{\frac{\mathrm{d}t}{2\pi}} \exp\!\left(-\frac{(I - \langle x_\Phi\rangle_t)^2\,\mathrm{d}t}{2}\right),
\end{aligned} \tag{A.2.1}$$

and we end up with the Gaussian distribution, which resonates with Eq. (A.0.2).

A.3 Stochastic Schrödinger Equation

With the probability distribution for I (Eq. (A.2.1)), we can easily calculate the normalization constant for one time step,

$$\begin{aligned}
1 =& \sqrt{\langle\psi_{\boldsymbol{I}}(t+\mathrm{d}t)|\psi_{\boldsymbol{I}}(t+\mathrm{d}t)\rangle} \\
=& \sqrt{\frac{\langle\psi_{\boldsymbol{I}}(t)|\, M_I^\dagger(t+\mathrm{d}t\,,t) M_I(t+\mathrm{d}t\,,t)\,|\psi_{\boldsymbol{I}}(t)\rangle}{N^2}} \\
=& \frac{\sqrt{\langle M_I^\dagger(t+\mathrm{d}t\,,t) M_I(t+\mathrm{d}t\,,t)\rangle_t}}{N} \\
=& \frac{\sqrt{\Pr([I],t+\mathrm{d}t)}}{N} \\
\Rightarrow N =& \sqrt[4]{\frac{\mathrm{d}t}{2\pi}} \exp\left(-\frac{\left(I-\sqrt{\kappa}\langle a+a^\dagger\rangle_t\right)^2 \mathrm{d}t}{4}\right).
\end{aligned} \tag{A.3.1}$$

Now, we have all the ingredients to derive the SSE, using Eq. (2.2.1) to connect the state $|\psi(t+\mathrm{d}t)\rangle$ with $|\psi(t+\mathrm{d}t)\rangle$ and secondly inserting Eq. (A.1.1) and Eq. (A.3.1). Afterwards, we expand the appearing exponentials with Eq. (A.0.4), multiply out all the terms and replace I with Eq. (A.0.2) to arrive at the SSE (Eq. (2.2.6)).

$$\begin{aligned}
\mathrm{d}|\psi(t)\rangle =& |\psi(t+\mathrm{d}t)\rangle - |\psi(t)\rangle \\
=& \left\{\frac{M_I(t+\mathrm{d}t\,,t)}{N} - \mathbb{1}\right\}|\psi(t)\rangle \\
=& \left\{\exp\left(\frac{\left(I-\sqrt{\kappa}\langle a+a^\dagger\rangle_t\right)^2 \mathrm{d}t}{4}\right)\exp\left(-\frac{I^2\,\mathrm{d}t}{4}\right)\right. \\
& \left.\times\left(\mathbb{1} - \left[iH(t) - I\sqrt{\kappa}a + \frac{\kappa}{2}a^\dagger a\right]\mathrm{d}t\right) - \mathbb{1}\right\}|\psi(t)\rangle \\
=& \left\{\exp\left(\frac{\left(-2\sqrt{\kappa}\langle a+a^\dagger\rangle_t I + \kappa\langle a+a^\dagger\rangle_t^2\right)\mathrm{d}t}{4}\right)\right. \\
& \left.\times\left(\mathbb{1} - \left[iH(t) - I\sqrt{\kappa}a + \frac{\kappa}{2}a^\dagger a\right]\mathrm{d}t\right) - \mathbb{1}\right\}|\psi(t)\rangle \\
=& \left\{\left(1 - \frac{\sqrt{\kappa}}{2}\langle a+a^\dagger\rangle_t I\,\mathrm{d}t + \frac{\kappa}{8}\langle a+a^\dagger\rangle_t^2 (I\,\mathrm{d}t)^2\right)\left(1+\frac{\kappa}{4}\langle a+a^\dagger\rangle_t^2\,\mathrm{d}t\right)\right. \\
& \left.\times\left(\mathbb{1} - \left[iH(t) - I\sqrt{\kappa}a + \frac{\kappa}{2}a^\dagger a\right]\mathrm{d}t\right) - \mathbb{1}\right\}|\psi(t)\rangle \\
=& \left\{\left(1 - \frac{\sqrt{\kappa}}{2}\langle a+a^\dagger\rangle_t I\,\mathrm{d}t + \frac{3}{8}\kappa\langle a+a^\dagger\rangle_t^2\,\mathrm{d}t\right)\right. \\
& \left.\times\left(\mathbb{1} - \left[iH(t) - I\sqrt{\kappa}a + \frac{\kappa}{2}a^\dagger a\right]\mathrm{d}t\right) - \mathbb{1}\right\}|\psi(t)\rangle
\end{aligned}$$

$$
\begin{aligned}
=&\Bigg\{-iH\,\mathrm{d}t-\frac{\kappa}{2}\left[a^\dagger a+\langle a+a^\dagger\rangle_t\,a-\frac{3}{4}\langle a+a^\dagger\rangle_t^2\right]\mathrm{d}t\\
&\qquad+\sqrt{\kappa}\left[a-\frac{1}{2}\langle a+a^\dagger\rangle_t\right]I\,\mathrm{d}t\Bigg\}\,|\psi(t)\rangle\\
=&\Bigg\{-iH\,\mathrm{d}t-\frac{\kappa}{2}\left[a^\dagger a-a\langle a+a^\dagger\rangle_t+\frac{1}{4}\langle a+a^\dagger\rangle_t^2\right]\mathrm{d}t\\
&\qquad+\sqrt{\kappa}\left[a-\frac{1}{2}\langle a+a^\dagger\rangle_t\right]\mathrm{d}W(t)\Bigg\}\,|\psi(t)\rangle
\end{aligned}
\tag{A.3.2}
$$

This is the stochastic Schrödinger equation we are using for the simulation.